RSC Advances

PAPER

View Article Online
View Journal | View Issue

Cite this: *RSC Adv.*, 2022, **12**, 7883

Tunable multicolor and bright white emission in PEG modified β-$NaGdF_4$ nanocrystals by systematic introduction of Ce^{3+} and Mn^{2+}/Ln^{3+}†

Xiaolong Li, *[a] Yaru Pei,[a] Ruimei Liang,[a] Chao Qian[b] and Jinzeng Wang*[a]

Received 14th January 2022
Accepted 3rd March 2022

DOI: 10.1039/d2ra00265e

rsc.li/rsc-advances

In this paper, Mn^{2+}/Ln^{3+}-doped hexagonal phase (β-) $NaGdF_4$:Ce (Ln = Tb, Dy, Eu) nanomaterials with subtly tuned multicolor output have been successfully synthesized by a typical simple hydrothermal method using polyethylene glycol (PEG) as a surface modifying agent. The crystal structures, morphology, luminescence performance, and energy transfer (ET) mechanism of the synthesized $NaGdF_4$ nanoparticles (NPs) were investigated in detail. It is found that due to the effective ET between Ce^{3+} and Mn^{2+}/Ln^{3+}, the multicolor down-conversion (DC) emission phosphors can yield three major emission bands in the visible region including blue, green and red. Moreover, the white emission could be realized through manipulating the doping ratio of Ce^{3+}, Dy^{3+} and Eu^{3+} with suitable concentration in β-$NaGdF_4$ NPs through effective resonance-type ET under the irradiation of 273 nm. And the corresponding CIE1931 coordinates were calculated to be (0.31, 0.32), which is near the normative white emission (0.33, 0.33). All the multicolor tuning and white emission results evidently suggest that the present Ce^{3+} and Mn^{2+}/Ln^{3+}-doped β-$NaGdF_4$ NPs are feasible phosphors for potential applications in white-light emitters, full-color displays and photonic devices.

1. Introduction

Features including color output, narrow emission peaks, and long fluorescence of lanthanide (Ln)-doped NPs have attracted much attention for their extensive applications in many fields, like as biological labels/images, drug delivery and light emitting devices.[1–8] During the past decades, the rare-earth (RE) ion doped fluorides have been used as wonderful host materials for both upconversion (UC) and DC have conceivable advantages over the conventional oxide materials because of their unique merits such as longer lifetime, higher light emission and lower phonon energy.[9–14] Among the RE fluoride nanomaterials, Ln-doped $NaGdF_4$ NPs with excellent optical and magnetic properties have been widely studied.[15–19] On the one hand, $NaGdF_4$ can act as an ideal host material due to Gd ions playing a crucial part in the ET mechanism serving as a bridge between the Ln^{3+} ions, consequently facilitating the ET process.[20,21] Moreover, Ln-doped $NaGdF_4$ NPs could show efficient DC emission excited by ultraviolet (UV) light when doping with Tb, Eu or Dy, while doping with another Ln^{3+} ion (*e.g.* Yb, Er, Tm) shows bright UC emission under the near-infrared excitation at 980 nm.[19,22,23] Based on the special merits, dual-mode fluorescent emission of Ln-doped $NaGdF_4$ NPs with core/shell structures have been synthesized reasonably by many researchers.[16,17,24] For example, Chen's group has proposed a protocol to fabricate UC and DC dual-mode luminescent $NaGdF_4$ NPs, which are composed of core ($NaGdF_4$:Yb^{3+}, Tm^{3+}) and shell ($NaGdF_4$:Eu^{3+}).[25] Furthermore, the seven unpaired electrons of Gd can produce the large magnetic dipole moment, which has ensured the materials containing Gd element could serve as the excellent agents in magnetic resonance image (MRI).[26,27] Li's team successfully synthesized $Tm^{3+}/Yb^{3+}/Er^{3+}$ co-doped $NaGdF_4$ NPs applied as MRI contrast agents.[17] Since multifarious researchers have done excellent works on the $NaGdF_4$ host because of such many unexceptionable merits mentioned all above.[28–32] However, it is still meaningful to explore an effective and facile approach to synthesize hydrophilic $NaGdF_4$ NPs doping with Mn^{2+} and Ln^{3+} for multicolor tunable emission, especially for white emission.

In this paper, the tunable DC luminescent $NaGdF_4$:Ce/Mn and Ce/Ln NPs (Ln = Tb, Eu, Dy) with PEG modified were successfully synthesized and the optical properties were studied in detail. The crystalline phase and morphology size of the as-prepared samples were successfully characterized, respectively. What's more, the luminescence properties including excitation/emission spectra of different Mn^{2+} and Ln^{3+} doping $NaGdF_4$:Ce NPs were systematically demonstrated. Besides, the ET mechanism between Ce^{3+} and Mn^{2+}/Ln^{3+} in $NaGdF_4$ NPs was

[a]*Key Laboratory of Magnetic Molecules and Magnetic Information Materials of Ministry of Education, School of Chemistry and Materials Science, Shanxi Normal University, Taiyuan, 030031, China. E-mail: lixlck@sxnu.edu.cn*

[b]*School of Physics and Electronics, Key Laboratory of Low-dimensional Quantum Structures and Quantum Control of the Ministry of Education, Synergetic Innovation Center for Quantum Effects and Applications, Hunan Normal University, Changsha 410081, China*

† Electronic supplementary information (ESI) available. See DOI: 10.1039/d2ra00265e

further discussed in detail. The doughty DC emission including the white emission of $NaGdF_4$:Ce/Mn and Ce/Ln NPs not only provides an efficient way to get any colors but also proposes a general route for the development of DC white light applied in lighting and displays fields.

2. Experimental

2.1 Chemicals and materials

The $RECl_3 \cdot 6H_2O$ (RE = Gd, Ce, Tb, Dy, Eu) was purchased from Sigma-Aldrich. PEG (average molecular = 6000), ethylene glycol (EG, 99%), NaOH, $MnCl_2$ and NaF were purchased through Sinopharm Chemical Reagent Co., China.

2.2 Preparation of Mn^{2+}/Ln^{3+} doped $NaGdF_4$:Ce NPs

A series of water-soluble Ce^{3+}/Mn^{2+} and Ce^{3+}/Ln^{3+}-doped (L = Tb, Dy, Eu) β-$NaGdF_4$ NPs were synthesized by a facile one-pot hydrothermal procedure using PEG as stabilization agents.[33] In a typical procedure, 1 g of PEG was firstly added in 100 mL beaker containing 15 mL of EG under vigorously stirring and heated properly. Following, a total amount (1 mmol) of $LnCl_3$ and/or $MnCl_2$ with logically designed molar ratio was added into the mixture under continuous magnetic stirring for thirty minutes. 5 mL of EG was added again and followed by 4 mmol of NaF was added under the agitation. Twenty minutes later, the resulting solution was transferred into Teflon-lined autoclave. And then the system was maintained reaction at 200 °C for 12 hours. The as-prepared samples were washed with de-ionized water and absolute ethyl alcohol three times in sequence to remove PEG and other remnants, and obtained after separating by centrifugation with 8000 rpm.

2.3 Materials characterization

The phase structure of the synthetic β-$NaGdF_4$:20% Ce^{3+}/1% Mn^{2+} and β-$NaGdF_4$:20% Ce^{3+}/1% Eu^{3+} NPs were characterized by the X-ray powder diffraction (XRD) performed. The morphology, microstructure and chemical constitution of the synthetic samples were recorded by TEM (FEI, Tecnai F20) instrument. The Fourier transform infrared (FTIR) of surface ligands grafting on the β-$NaGdF_4$ NPs was detected *via* FTIR spectra using a Magna 760 spectrometer (Nicolet). The DC excitation/emission spectra of the samples were examined by the Zolix spectrometers (fluoroSENS 9000A). The digital photographs of multicolor emission of the as-prepared powders were recorded by a Canon digital camera at room temperature.

3. Results and discussion

3.1 Morphology and microstructure

The high-quality of β-$NaGdF_4$:Ce NPs were synthesized with different ratio of Mn^{2+}/Ln^{3+} doping at the same condition. Fig. 1 shows the typical XRD patterns of the two representative as-prepared 1% Mn^{2+} and 1% Eu^{3+} doped $NaGdF_4$:20% Ce^{3+} NPs, respectively. The strong and sharp diffraction peaks of the synthetic NPs, as shown in the Fig. 1, can be exactly assigned to the pure β-$NaGdF_4$ with the standard XRD pattern (JCPDS file number: 27-0699). No other impurity diffraction peaks have examined in the XRD patterns, indicating that the pure phase and high crystalline of the $NaGdF_4$ NPs could be obtained *via* hydrothermal method at low temperature (200 °C). With further increasing the contents of Mn^{2+} to 5% and 10%, the crystal phase of the as-prepared NPs was still matched well with hexagonal phase structure (Fig. S1†). In addition, the pure hexagonal phase $NaGdF_4$ has a space group of *P*6 and refined cell parameters of $a = b = 6.020$ Å, $c = 3.601$ Å, $V = 113.02$ Å^3 and $Z = 1.5$, which were essential and important factors in further investigates the multicolor performance and ET mechanism of Ce^{2+}/Mn^{2+} and Ce^{3+}/Ln^{3+} doped in the $NaGdF_4$ NPs.

The morphologies of the prepared β-$NaGdF_4$:20% Ce^{3+}/1% Mn^{2+} and $NaGdF_4$:20% Ce^{3+}/1% Eu^{3+} NPs were illustrated by the TEM assay. As shown in the Fig. 2a and b, the as-prepared $NaGdF_4$ NPs present uniform near-spherical structure and no other impurity nanostructure were observed. The size distribution based on the TEM image (Fig. 1a) was measured to be about 34.7 ± 3.43 nm (Fig. S2†). To further disclose the structure of the two obtained NPs, the distance between the adjacent lattice fringes with a measured d-spacing of 0.298 nm (inset of Fig. 2a) was observed, which is well matched with the plane (110) of β-$NaGdF_4$. While the inset image in the Fig. 2b shows the lattice distance of 0.531 nm, which is corresponding to d-spacing for the (100) plane of the β-$NaGdF_4$ structure. In addition, the obvious lattice fringes in high resolution TEM (HRTEM) images confirm the high crystallinity of the synthetic samples and also corroborate these ions doping having no influence on the phase of $NaGdF_4$ NPs. The surface functionalization of the $NaGdF_4$ NPs was recorded by FTIR spectrum (Fig. S3†). The peaks centered at 3454, 2896, 1651, 1513, and 1091 cm^{-1} are corresponded to O–H, –CH_2, C–O, –COO^-, C–O–C, respectively, indicating the PEG successful coating on the surface of the $NaGdF_4$ NPs. Furthermore, the selected area electron diffraction (SAED) in the Fig. 2c clearly presents the intense diffraction fringes, which could be ascribed to the specific (102), (201), (111), (110) and (100) planes of the β-$NaGdF_4$, also coincided well with the former XRD analysis results. To confirm the comprise elements of the DC samples,

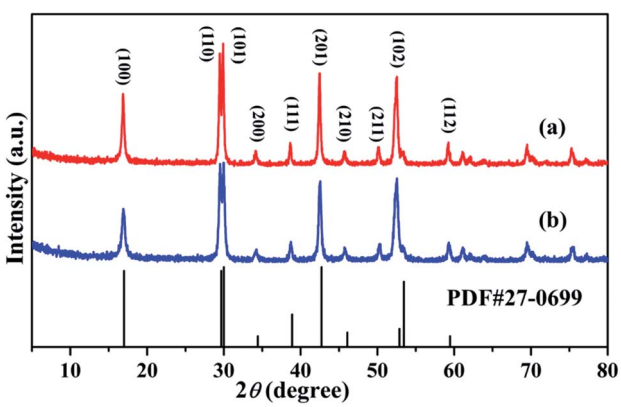

Fig. 1 The XRD patterns of (a) 1% Mn^{2+} and (b) 1% Eu^{3+} doping of $NaGdF_4$:20% Ce^{3+} NPs and the standard card of hexagonal phase $NaGdF_4$ crystal (JCPDS no. 27-0699).

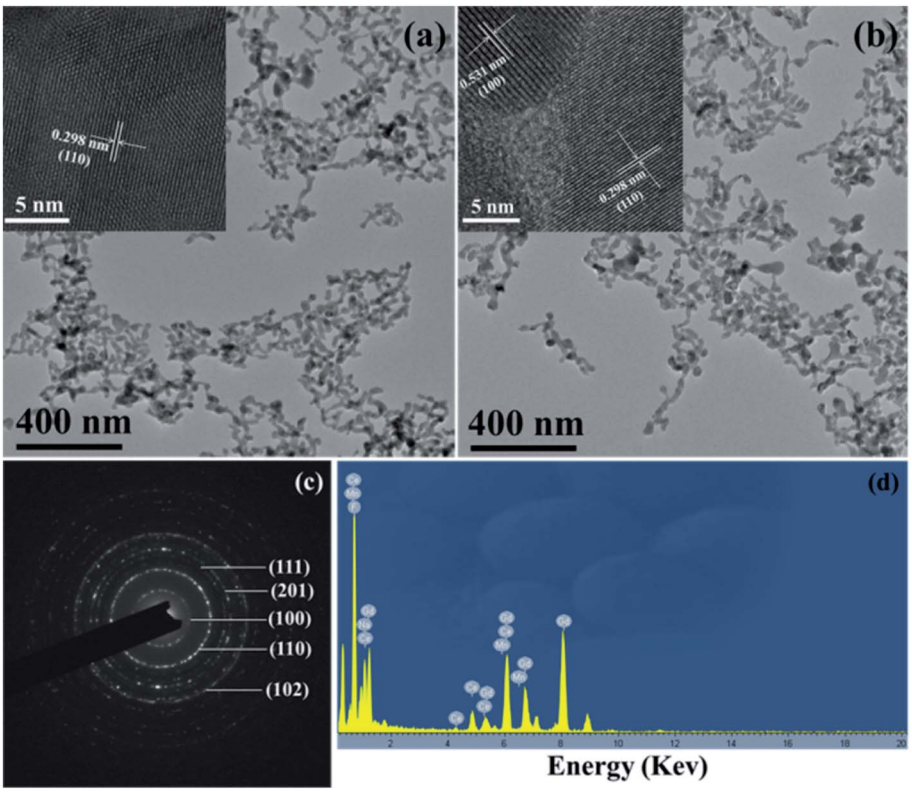

Fig. 2 TEM and HRTEM images of (a) 1% Mn^{2+} and (b) 1% Eu^{3+} doping β-$NaGdF_4$:20% Ce^{3+} NPs. (c) The SAED pattern of the sample of (a). (d) Typical EDS spectrum of β-$NaGdF_4$:20% Ce^{3+}/1% Mn^{2+} samples.

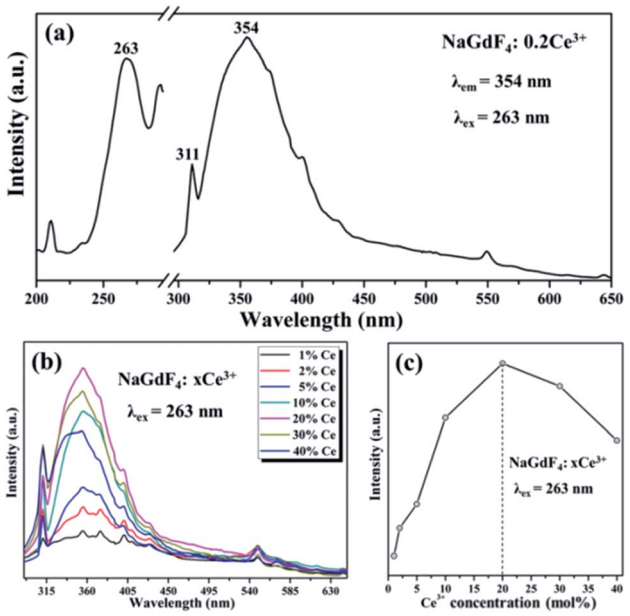

Fig. 3 (a) Excitation and emission spectrum of the $NaGdF_4$:20% Ce^{3+} sample. (b) Emission spectra of the $NaGdF_4$:$x$$Ce^{3+}$ (x = 1, 2, 5, 10, 20, 30 and 40 mol%) NPs. (c) PL intensity of $NaGdF_4$:$x$$Ce^{3+}$ samples with the Ce^{3+} concentration.

the typical EDS spectrum of 20% Ce^{3+} and 1% Mn^{2+} doped β-$NaGdF_4$ NPs were carried out. The result reveals that the as-prepared NPs are principally composed of Cu, C, Gd, Ce, Mn, Na and F elements, indicating that the Mn^{2+} and Ce^{3+} were successfully doped into the $NaGdF_4$ host. Note that the signals of Cu and C are resulting from copper grid and the carbon film on the supporting copper, respectively.

3.2 Optical properties and ET mechanism

To reveal the DC emission properties of the preparative samples, the DC excitation and emission spectra were systematically recorded. Fig. 3 shows the PL properties of only Ce^{3+} doped in $NaGdF_4$ NPs. The excitation spectrum of $NaGdF_4$:20% Ce^{3+} samples monitored at 354 nm shows a strong broad band at 263 nm because of the lowest Ce^{3+} 4f → 5d transition (left of Fig. 3a).[34] The emission spectrum was recorded under the excitation wavelength at 263 nm at room temperature, obviously with a wave band ranging from 305 nm to 450 nm including the maximum at about 354 nm and the sharp line at about 311 nm. The maximum and sharp peaks were due to energy efficient transition from the $5d_1$ to $4f_1$ of Ce^{3+} and $^6P_{7/2} \rightarrow {}^8S_{7/2}$ electron transition of Gd^{3+}, respectively (right of Fig. 3a). The relative emission intensities in $NaGdF_4$ NPs can be precisely changed by tuning the sensitizer doping concentration. By adjusting the different Ce^{3+} (from 1 to 40 mol%) concentrations, the optimum doping concentration of Ce^{3+} in β-$NaGdF_4$ can be precisely obtained. As shown in Fig. 3b, Ce^{3+} doped $NaGdF_4$ NPs exhibits the almost same emission peeks but different emission intensity with varying Ce^{3+} doping concentration. It is worth noting that the PL emission intensity remarkably enhanced firstly and

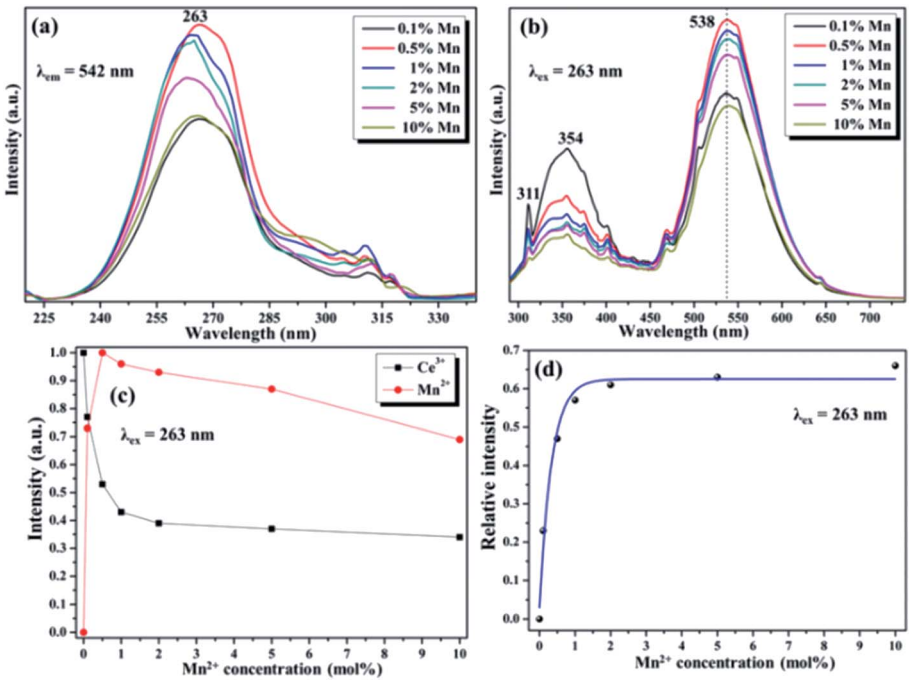

Fig. 4 (a) Excitation and (b) emission spectra of $NaGdF_4$:20% Ce^{3+}/xMn^{2+} ($x = 0.1$, 0.5, 1, 2, 5 and 10 mol%) samples. (c) The PL intensity curves of $NaGdF_4$:Ce^{3+}/Mn^{2+} samples monitored at 354 nm of Ce^{3+} emission and 538 nm of Mn^{2+} emission as a function of the Mn^{2+} doping concentration. (d) ET efficiency from Ce^{3+} to Mn^{2+} in $NaGdF_4$:20% Ce^{3+}/xMn^{2+} samples.

then decreased with a further increase of doping concentration, reaching a maximum at 20% of Ce^{3+} doping concentration under excited at 263 nm. The emission intensity changes with variations of Ce^{3+} are directly observed from Fig. 3c.

The results demonstrated that the optimum doping concentration of Ce^{3+} would be 20% in the $NaGdF_4$ host on account of the concentration quenching effect.[35] Therefore, based on the Blasse's report, the critical distance (R_C) of Ce^{3+} ions in $NaGdF_4$ host could be calculated by the concentration quenching method:[36]

$$R_C \approx 2\left[\frac{3V}{4\pi X_C N}\right]^{1/3} \quad (1)$$

where V, N and X_C are the volume, number of host cations and optimum concentration of doped ions of the unit cell, respectively. All of above parameters of Ce^{3+} in the $NaGdF_4$ host are as follows, $V = 113.02$ Å^3, $N = 1.5$ and $X_C = 0.2$; therefore, R_C is about 8.96 Å calculated by using eqn (1).

To further invested the ET mechanism among Ce^{3+} and Mn^{2+}/Tb^{3+}/Eu^{3+}/Dy^{3+} in $NaGdF_4$ host, the PL emission performance of Mn^{2+}/Tb^{3+}/Eu^{3+}/Dy^{3+} co-/doped $NaGdF_4$:20% Ce NPs have been studied, respectively. The various excitation/emission spectra of the $NaGdF_4$:20% Ce with a variety of Mn^{2+} doping concentration turning from 0 to 10 mol% were monitored at 542 nm and excited by 263 nm UV light, respectively. As demonstrated in the Fig. 4a, the excitation spectra show peeks range from 230 nm to 310 nm and reach a maximum value at 263 nm, which is ascribed to the 4f → 5d electron transition of Ce^{3+}. The emission spectra of different Mn^{2+} with fixed Ce^{3+}(20%) co-doped $NaGdF_4$ (Fig. 4b) show the broad emission

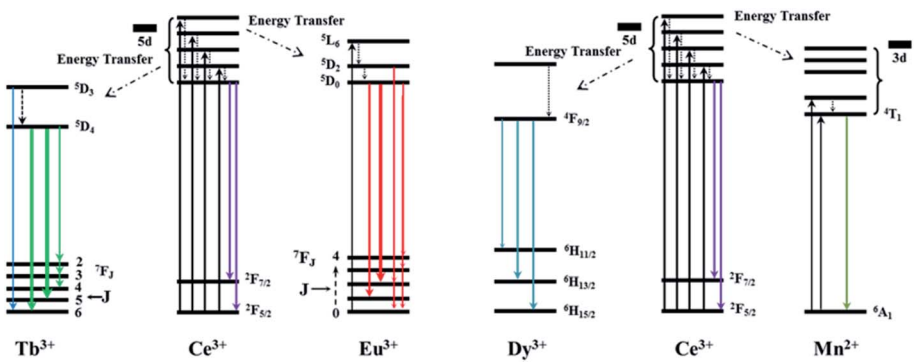

Fig. 5 The proposed ET mechanism for Ce^{3+}/Tb^{3+}, Ce^{3+}/Eu^{3+}, Ce^{3+}/Dy^{3+} and Ce^{3+}/Mn^{2+} in the $NaGdF_4$ host.

band were centered at 354 nm and 538 nm, which are respectively attributed to the electrons transition with $5d_1 \rightarrow 4f_1$ of Ce^{3+} and $^4T_1 \rightarrow {}^6A_1$ of Mn^{2+}, respectively.[37] Note that, the sharp peak (311 nm) resulting from $^6P_{7/2} \rightarrow {}^8S_{7/2}$ transitions of Gd^{3+} was continuously decreased with the augment of Mn^{2+} concentration under the excitation, indicating that the effective ET between Gd^{3+} and Mn^{2+} was exist in $NaGdF_4$ host. Moreover, the emission intensity of Ce^{3+} was continuously decreased, while the intensity of Mn^{2+} emission increased firstly and then decreased with the increase of Mn^{2+} concentration. The corresponding PL emission intensity of the $NaGdF_4$:20% Ce^{3+}/Mn^{2+} system was shown in the Fig. 4c. The initial Mn^{2+} emission intensity increase demonstrates an effectual ET between Ce^{3+} and Mn^{2+}, while the latter decrease was because of the concentration quenching effect in the $NaGdF_4$:20% Ce^{3+}/Mn^{2+} system.[38] And the ET efficiency (η_T) could be estimated by the followed formula:[39]

$$\eta_T = 1 - \frac{I_S}{I_{S0}} \quad (2)$$

where η_T is ET efficiency between Ce^{3+} and Mn^{2+}. I_S and I_{S0} are the PL intensity of a sensitizer (Ce^{3+}) doped with and without of an activator (Mn^{2+}), respectively. The η_T value curve of different Mn^{2+} concentration doped $NaGdF_4$:20% Ce calculated by eqn (2) was fitted using a bi-exponential function. The calculated results presented in the Fig. 4d, which clearly revel that the η_T was increase rapidly and then slow down gradually and the maximum can reach to 63% with the continuing Mn^{2+} concentration increase under the 263 nm excitation. The η_T value further demonstrates the efficient ET from Ce^{3+} to Mn^{2+} in $NaGdF_4$ system. The possible ET mechanism of the $NaGdF_4$:20% Ce^{3+}/Mn^{2+} was shown in the Fig. 5. The R_C between Ce^{3+} and Mn^{2+} ions also could be estimated by the concentration quenching method mentioned in eqn (1). The difference is that X_C is the critical total concentration of rare earth ions including Ce^{3+} and Mn^{2+}. Therefore, the ET R_C between the Ce^{3+} and Mn^{2+} is about 30.66 Å based on concentration quenching eqn (1) when X_C equals 0.005, which is larger than 4 Å, revealing that the ET mechanism of Ce^{3+} and Mn^{2+} ions is maybe multipolar interaction.[37]

The fluorescence results of Ce^{3+}/Tb^{3+}, Ce^{3+}/Dy^{3+} and Ce^{3+}/Eu^{3+} doped in $NaGdF_4$ host based on the similar ET mechanism were shown in the Fig. 6, 7 and 8, respectively. Fig. 6a and b detailly illustrate the excitation/emission spectra of Ce/Tb co-doped $NaGdF_4$ host, which strongly indicate that the existence of ET from Ce^{3+} to Tb^{3+}. The typical emission peaks at 380 nm, 489 nm, 542 nm, 584 nm and 620 nm, which are respectively attributed to the $^5D_3 \rightarrow {}^7F_6$ and $^5D_4 \rightarrow {}^7F_J$ ($J = 6, 5, 4, 3$) electron transitions of Tb^{3+}.[37] The possible ET mechanism between Ce^{3+} and Tb^{3+} were also shown in the Fig. 5. The corresponding PL emission intensity of Ce^{3+} and Tb^{3+} in the $NaGdF_4$ host was demonstrated in the Fig. 6c. It is clearly present that the intensity of emission band (300–400 nm) of Ce^{3+} was decreasing all the way while the emission intensity of Tb^{3+} increased at first and then decreased with the continuous increase of Tb^{3+}. The change of PL intensity of Ce^{3+} and Tb^{3+} directly illustrates the efficient ET from Ce^{3+} to Tb^{3+} in $NaGdF_4$ host. The ET efficiency (η_T) was calculated by eqn (2), the maximum value of η_T is about

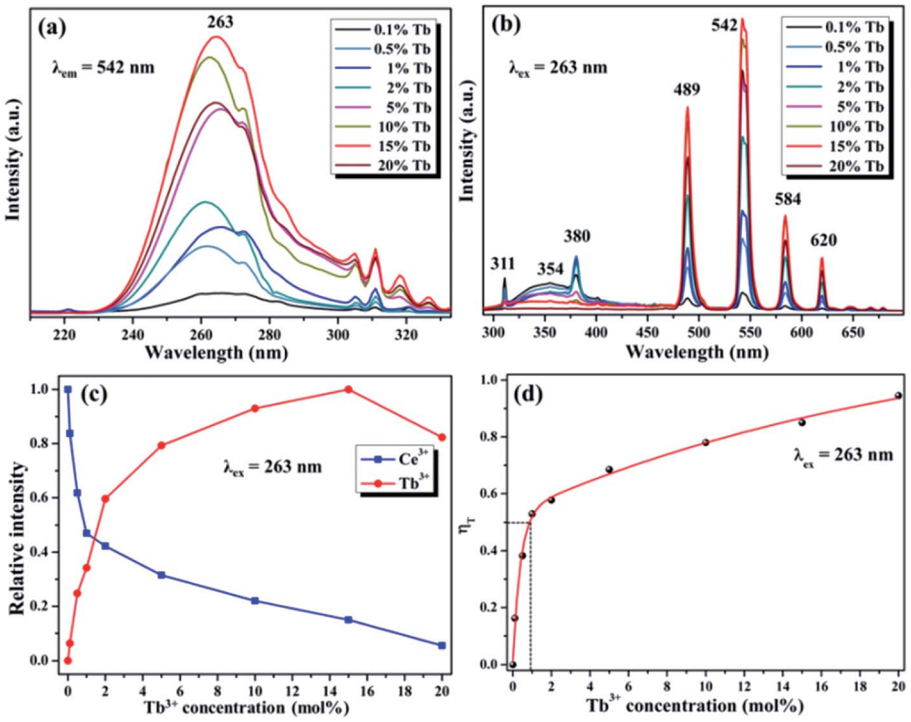

Fig. 6 (a) Excitation and (b) emission spectra of the $NaGdF_4$:20% Ce^{3+}/xTb^{3+} ($x = 0.1$, 0.5, 1, 2, 5, 10, 15 and 20 mol%) samples. (c) PL intensity curves of $NaGdF_4$:Ce^{3+}/Tb^{3+} samples monitored at 354 nm of Ce^{3+} emission and 542 nm of Tb^{3+} emission variation curve with the Tb^{3+} doping. (d) ET efficiency from Ce^{3+} to Tb^{3+} in $NaGdF_4$ host.

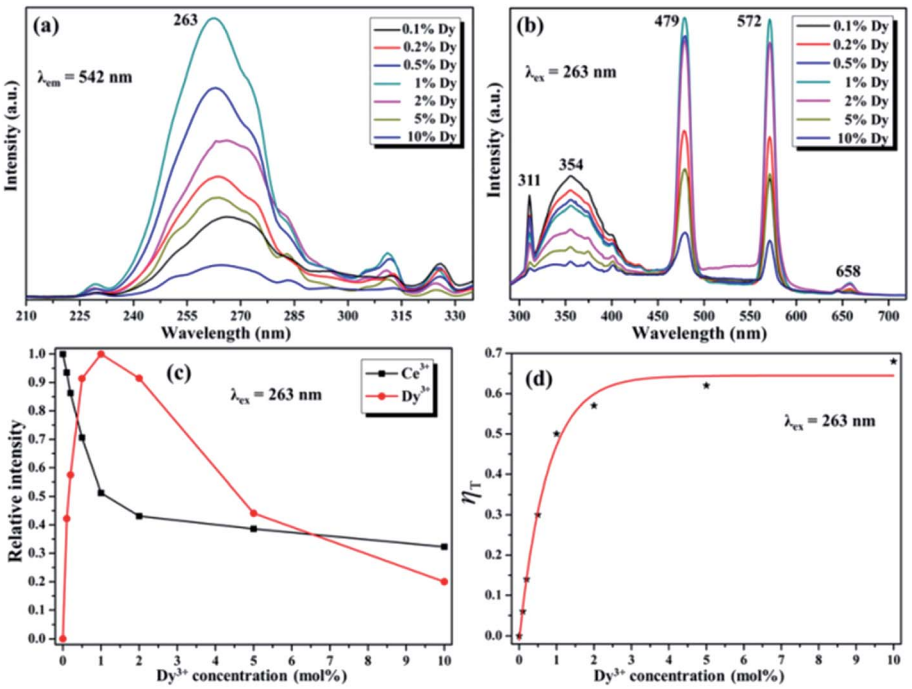

Fig. 7 (a) Excitation and (b) emission spectra of the $NaGdF_4$:20% Ce^{3+}/xDy^{3+} (x = 0.1, 0.2, 0.5, 1, 2, 5 and 10 mol%) samples. (c) PL intensity curves of $NaGdF_4$:20% Ce^{3+}/xDy^{3+} samples monitored at 354 nm of Ce^{3+} emission and 572 nm of Dy^{3+} emission as a function of the Dy^{3+} doping concentration. (d) ET efficiency from Ce^{3+} to Dy^{3+} in $NaGdF_4$ host.

94% as represented in the Fig. 6d. The ET R_C between Ce^{3+} and Tb^{3+} is computed to be 9.86 Å larger than 4 Å, indicating that the ET mechanism from Ce^{3+} to Tb^{3+} ions is also multipolar interaction.[40]

Fig. 7a and b demonstrate the excitation/emission spectra of Ce/Dy co-doped in $NaGdF_4$ NPs. As shown in the Fig. 7b, the emblematic emission peaks at 479 nm and 512 nm are appeared, which is due to the electron transitions of $^4F_{9/2} \rightarrow {}^6H_{15/2}$ and $^4F_{9/2} \rightarrow {}^6H_{13/2}$ of Dy^{3+}. Fig. 5 also shows the corresponding ET mechanism among Ce^{3+} and Dy^{3+}. From the PL intensity of Ce^{3+}/Dy^{3+} in the Fig. 7c, it can be seen that the intensity of Ce^{3+} and Dy^{3+} emission is obviously different. The intensity of Ce^{3+} emission was decreased but that of Dy^{3+} emission was increased firstly. With the continue increase of doping concentration of Dy^{3+}, the intensity of Ce^{3+} emission was still decreased while Dy^{3+} emission is decrease on the contrary. All of the results strongly validate the effective ET from the Ce^{3+} to Dy^{3+} in $NaGdF_4$ NPs. The value of η_T calculated by eqn (2) were shown in the Fig. 7d and the maximum is about 65%. The R_C of ET from the Ce^{3+} to Dy^{3+} estimated using eqn (1) is about 24.32 Å when X_C equals 0.01.

Fig. 8a demonstrates the excitation spectra of $NaGdF_4$:20% Ce/Eu NPs and the corresponding emission spectra was shown in the Fig. 8b. The representative emission band were centered at 591 nm and 615 nm, ascribed to the $^5D_0 \rightarrow {}^7F_1$ and $^5D_0 \rightarrow {}^7F_2$ electron transition of Eu^{3+}, which was combined with the corresponding ET mechanism with Ce^{3+} and Eu^{3+} in the Fig. 5. The whole PL emission results dependent on the different doping concentration of Eu^{3+} were performed to validate the efficient ET between Ce^{3+} and Eu^{3+}. As shown in Fig. 8c and d, with continuously increasing Eu^{3+} concentration, the emission intensity of Ce^{3+} decreased while Eu^{3+} was increased firstly and then decreased, which may because of the concentration quenching effect. These results also indicate the resultful ET between the Ce^{3+} and Eu^{3+} in $NaGdF_4$ NPs. The η_T was also calculated by eqn (2), the results of η_T value were shown in the Fig. 8d and the maximum is about 75%. The R_C of ET from the Ce^{3+} to Eu^{3+} is determined by the concentration quenching equation to be 24.32 Å.

Due to the wide range-tunable emissions of Ce^{3+}/Dy^{3+} and Ce^{3+}/Eu^{2+} doped $NaGdF_4$ NPs, it is reasonable to design the sensitizer (Ce^{3+}) and activator (Dy^{3+}, Eu^{3+}) tri-doping $NaGdF_4$ NPs for precisely control emission, especially for white emission. Therefore, the different doping concentration of Eu^{3+} in the $NaGdF_4$:20% Ce/1% Dy NPs were further synthesized for systematic white emission research. As shown in Fig. 9a, the $NaGdF_4$ NPs tri-doped with Ce^{3+}/Dy^{3+}(20/1 mol%) and Eu (x mol%) exhibit the characteristic sharp emission peaks corresponded to the green, blue and red emissions, which can be attributed to the efficient emission of Ce^{3+}, Dy^{3+} and Eu^{3+}. With the continuous increase doping of Eu^{3+}, the emission intensity of Ce^{3+} and Dy^{3+} ions was always decreased, while the emission intensity of Eu^{3+} can reach the maximum at the concentration of 0.5% (Fig. 9b). It can be proved that the efficient ET between Ce^{3+} and Eu^{3+} ions is more significant at the coexistence of Dy^{3+}/Eu^{3+}. According to the calculation of emission spectrum data by using the color coordinate calculation soft-ware, the color of the emission light is closest to white when the Eu^{3+} ion doping concentration is 0.5 mmol%. The corresponding emissive spectrum is obviously exhibited in the Fig. 9c. Fig. 9d shows the

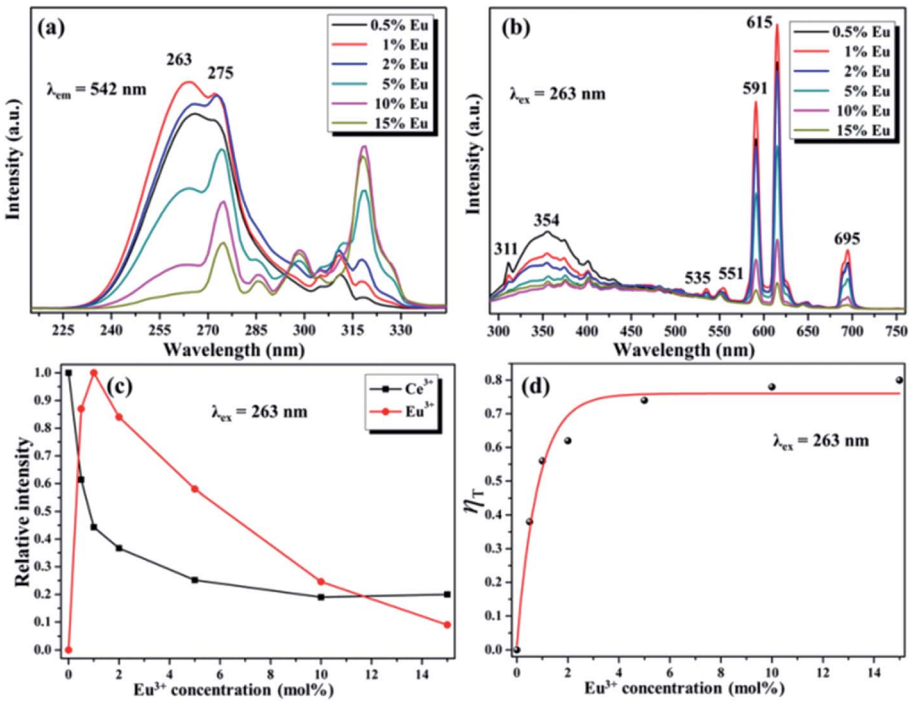

Fig. 8 (a) Excitation and (b) emission spectra of 20% Ce^{3+}/xEu^{3+} (x = 0.5, 1, 2, 5, 10 and 15 mol%) $NaGdF_4$ samples. (c) PL intensity curves of $NaGdF_4$:20% Ce^{3+}/xTb^{3+} samples monitored at 354 nm of Ce^{3+} emission and 615 nm of Eu^{3+} emission as a function of the Eu^{3+} doping concentration. (d) ET efficiency from Ce^{3+} to Eu^{3+} in $NaGdF_4$ samples.

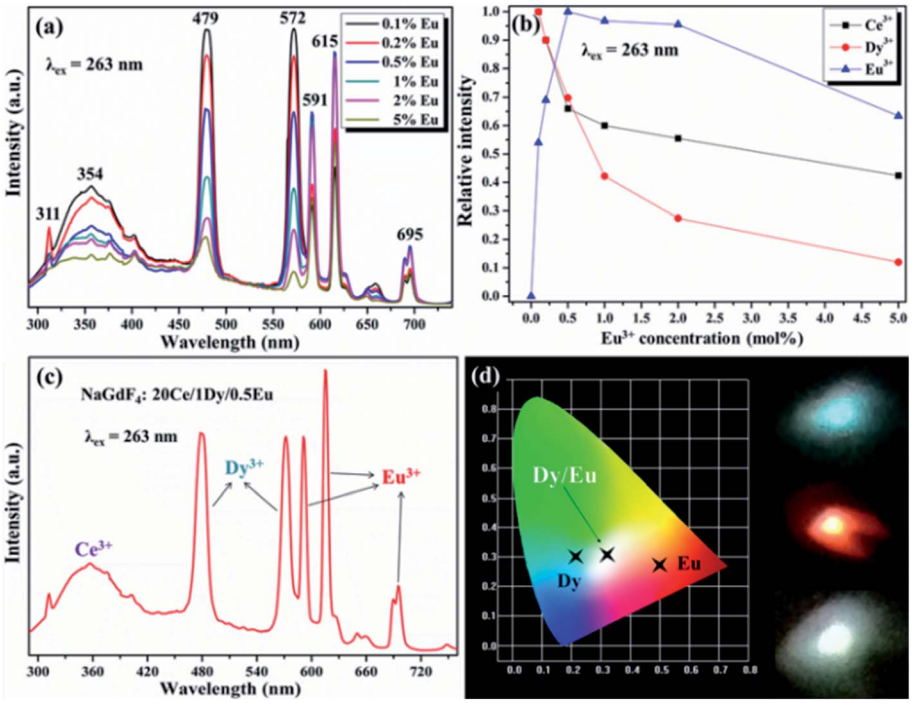

Fig. 9 (a) Emission spectra of the $NaGdF_4$:20% Ce^{3+}/1% Dy^{3+}/xEu^{3+} (x = 0.1, 0.2, 0.5, 1, 2 and 5%) samples. (b) The corresponding PL intensity curves of $NaGdF_4$:20% Ce^{3+}/1% Dy^{3+}/xEu^{3+} samples monitored at 354 nm of Ce^{3+} emission, 572 nm of Dy^{3+} emission and 615 nm of Eu^{3+} emission as a function of the Eu^{3+} doping concentration. (c) Emission spectrum of the $NaGdF_4$:20% Ce^{3+}/1% Dy^{3+}/0.5% Eu^{3+} samples. (d) CIE chromaticity diagram of $NaGdF_4$:20% Ce^{3+} NPs doped with 1% Dy^{3+}, 1% Eu^{3+} and 1% Dy^{3+}/0.5% Eu^{3+}, the insets are corresponding photographs of these NPs under 263 nm UV light.

color coordinate diagram of Dy^{3+} and Eu^{3+} single and co-doped in $NaGdF_4$:20% Ce host and the corresponding luminescence photos are demonstrated on the right. It can be clearly seen that the white emission of $NaGdF_4$:20% Ce NPs is successfully realized when doping with 1% Dy^{3+} and 0.5% Eu^{3+}. The CIE chromaticity coordinates were computed about (0.31, 0.32) according to the emission spectrum, which is near closely to the standard white emission (0.33, 0.33).

4. Conclusion

In summary, a series of hydrophilic $NaGdF_4$:Ce/Mn and Ce/Ln (Ln = Tb, Dy, Eu) NPs with multicolor tunable emission have been successfully fabricated. The morphology studied displays the successful manufacture of the high-quality $NaGdF_4$ NPs with uniform shape, mono-dispersity and pure hexagonal phase. Through adjusting the doping ions and content, the relative emission intensities of various emission colors can be adjusted precisely, resulting in the multicolor emission. Furthermore, based on the acquirement of the three basic colors (blue, green and red) in the Ln-doped $NaGdF_4$ system, the boosting white emissions could be obtained naturally with emission balance due to the effective ET from Ce^{3+} to Eu^{3+}/Dy^{3+}. It is importantly elucidated that the CIE coordinates of $NaGdF_4$:20% Ce^{3+}/1% Dy^{3+}/0.5% Eu^{3+} NPs are seated in the white region and calculated to be (0.31, 0.32), which is near closely to the normative white light emission (0.33, 0.33). The white emission in $NaGdF_4$ host by tri-doping Ce^{3+}, Dy^{3+} and Eu^{3+} was achieved for the first time. The excellent DC emission, variable multicolor output and lightful white luminescence of the Mn^{2+}/Ln^{3+}-doped $NaGdF_4$:Ce NPs may have potential applications in diverse fields.

Conflicts of interest

There are no conflicts to declare.

Acknowledgements

This work was supported by the National Natural Science Foundation of China (No. 52003144), and the Youth Science Foundation of Shanxi Province (No. 201901D211401).

Notes and references

1 X. Qin, X. W. Liu, W. Huang, M. Bettinelli and X. G. Liu, *Chem. Rev.*, 2017, **117**, 4488–4527.
2 F. Wang and X. G. Liu, *Chem. Soc. Rev.*, 2009, **38**, 976–989.
3 S. Wu, D. J. Milliron, S. Aloni, V. Altoea, D. V. Talapin, B. E. Cohen and P. J. Schuck, *Proc. Natl. Acad. Sci. U. S. A.*, 2009, **106**, 10917–10921.
4 M. An, J. Cui, Q. He and L. Wang, *J. Mater. Chem. B*, 2013, **1**, 1333–1339.
5 J. W. Stouwdam, G. A. Hebbink, J. Huskens and F. C. J. M. van Veggel, *Chem. Mater.*, 2003, **15**, 4604–4616.
6 G. A. Kumar, C. W. Chen, J. Ballato and R. E. Riman, *Chem. Mater.*, 2007, **19**, 1523–1528.
7 H. Wang, X. D. Hong, R. L. Han, J. H. Shi, Z. J. Liu, S. J. Liu, Y. Wang and Y. Gan, *Sci. Rep.*, 2015, **5**, 17088–17093.
8 F. Wang, D. Banerjee, Y. S. Liu, X. Y. Chen and X. G. Liu, *Analyst*, 2010, **135**, 1839–1854.
9 X. Bai, D. Li, Q. Liu, B. Dong, S. Xu and H. W. Song, *J. Mater. Chem.*, 2012, **22**, 24698–24704.
10 F. Meiser, C. Cortez and F. Caruso, *Angew. Chem., Int. Ed.*, 2004, **43**, 5954–5957.
11 Z. L. Wang, Z. W. Quan, P. Y. Jia, C. K. Lin, Y. Luo, Y. Chen, J. Fang, W. Zhou, C. J. O' Connor and J. Lin, *Chem. Mater.*, 2006, **18**, 2030–2037.
12 F. Wang and X. G. Liu, *J. Am. Chem. Soc.*, 2008, **130**, 5642–5643.
13 C. Feldmann, M. Roming and K. Trampert, *Small*, 2006, **2**, 1248–1250.
14 G. S. Yi, H. C. Lu, S. Y. Zhao, Y. Ge, W. J. Yang, D. P. Chen and L. H. Guo, *Nano Lett.*, 2004, **4**, 2191–2196.
15 Y. Wu, C. X. Li, D. M. Yang and J. Lin, *J. Colloid Interface Sci.*, 2011, **354**, 429–436.
16 Y. S. Liu, D. T. Tu, H. M. Zhu, R. F. Li, W. Q. Luo and X. Y. Chen, *Adv. Mater.*, 2010, **22**, 3266–3271.
17 J. Zhou, Y. Sun, X. X. Du, L. Q. Xiong, H. Hu and F. Y. Li, *Biomaterials*, 2010, **31**, 3287–3295.
18 H. Y. Xing, S. J. Zhang, W. B. Bu, X. P. Zheng, L. J. Wang, Q. F. Xiao, D. L. Ni, J. M. Zhang, L. P. Zhou, W. J. Peng, K. L. Zhao, Y. Q. Hua and J. L. Shi, *Adv. Mater.*, 2014, **26**, 3867–3872.
19 M. He, P. Huang, C. L. Zhang, H. Y. Hu, C. C. Bao, G. Gao, R. He and D. X. Cui, *Adv. Funct. Mater.*, 2011, **21**, 4470–4477.
20 F. Wang, X. P. Fan, M. Q. Wang and Y. Zhang, *Nanotechnology*, 2007, **18**, 025701.
21 C. H. Liu, H. Wang, X. R. Zhang and D. P. Chen, *J. Mater. Chem.*, 2009, **19**, 489–496.
22 C. Y. Liu, Z. Y. Gao, J. F. Zeng, Y. Hou, F. Fang, Y. L. Li, R. R. Qiao, L. Shen, H. Lei, W. S. Yang and M. Y. Gao, *ACS Nano*, 2013, **7**, 7227–7240.
23 J. Li, Z. D. Hao, X. Zhang, Y. S. Luo, J. H. Zhao, S. Z. Lu, J. Cao and J. H. Zhang, *J. Colloid Interface Sci.*, 2013, **392**, 206–212.
24 Y. I. Park, J. H. Kim, K. T. Lee, K. S. Jeon, H. B. Na, J. H. Yu, H. M. Kim, N. Lee, S. H. Choi, S. I. Baik, H. Kim, S. P. Park, B. J. Park, Y. W. Kim, S. H. Lee, S. Y. Yoon, I. C. Song, W. K. Moon, Y. D. Suh and T. Hyeon, *Adv. Mater.*, 2009, **21**, 4467–4471.
25 H. S. Jang, K. Woo and K. Lim, *Opt. Express*, 2012, **20**, 17107–17118.
26 X. W. Zhang, Z. Zhao, X. Zhang, D. B. Cordes, B. Weeks, B. Qiu, M. Kailasnath and D. K. Sardar, *Nano Res.*, 2014, **8**, 636–648.
27 Y. Wu, D. M. Yang, X. J. Kang, C. X. Li and J. Lin, *Mater. Res. Bull.*, 2013, **48**, 2843–2849.
28 L. L. Wang, L. L. Liu, Q. Xu, T. Sun and W. N. Gu, *Adv. Mater. Res.*, 2013, **661**, 74–78.
29 H. X. Guan, G. X. Liu, J. X. Wang, X. T. Dong and W. S. Yu, *Dalton Trans.*, 2014, **43**, 10801–10808.
30 X. Q. Zhang, X. P. Fan, X. S. Qiao and Q. Luo, *Mater. Chem. Phys.*, 2010, **121**, 274–279.

31 M. Karbowiak, A. Mech, A. Bednarkiewicz, W. Stręk and L. Kępińskib, *J. Phys. Chem. Solids*, 2005, **66**, 1008–1019.
32 B. F. Wang, R. R. Deng, J. Wang, Q. X. Wang, Y. Han, H. M. Zhu, X. Y. Chen and X. G. Liu, *Nat. Mater.*, 2011, **10**, 968–973.
33 S. J. Zeng, M.-K. Tsang, C.-F. Chan, K.-L. Wong and J. H. Hao, *Biomaterials*, 2012, **33**, 9232–9238.
34 T. Q. Sheng, Z. L. Fu, X. J. Wang, S. H. Zhou, S. Y. Zhang and Z. W. Dai, *J. Phys. Chem. C*, 2012, **116**, 19597–19603.
35 T. S. Chan, C. C. Lin, R. S. Liu, R. J. Xie, N. Hirosaki and B. M. Cheng, *J. Electrochem. Soc.*, 2009, **156**, J189–J191.
36 G. Blasse, *J. Solid State Chem.*, 1986, **62**, 207–211.
37 Y. Zhang, G. G. Li, D. L. Geng, M. M. Shang, C. Peng and J. Lin, *Inorg. Chem.*, 2012, **51**, 11655–11664.
38 G. G. Li, D. L. Geng, M. M. Shang, Y. Zhang, C. Peng, Z. Y. Cheng and J. Lin, *J. Phys. Chem. C*, 2011, **115**, 21882–21892.
39 W. J. Yang and T. M. Chen, *Appl. Phys. Lett.*, 2006, **88**, 101903.
40 T. W. Kuo and T. M. Chen, *J. Electrochem. Soc.*, 2010, **157**, 216–220.